Molecular Crystals and Liquid Crystals
Publication details, including instructions for authors and subscription information:
http://www.tandfonline.com/loi/gmcl16

Optical Study of a Chiral Smectic C Under Shear

Pawel Pierański [a], Etienne Guyon [a], Patrick Keller [a], Lionel Liébert [a], Wojciech Kuczyński [b] & Piotr Pierański [b]

[a] Laboratoire de Physique des Solides associé au CNRS, Université Paris-Sud, 91405, Orsay

[b] Physics Institute of Polish Academy of Sciences, Poznań, ul. Smoluchowskiego, 17/79

Version of record first published: 28 Mar 2007.

To cite this article: Pawel Pierański , Etienne Guyon , Patrick Keller , Lionel Liébert , Wojciech Kuczyński & Piotr Pierański (1977): Optical Study of a Chiral Smectic C Under Shear, Molecular Crystals and Liquid Crystals, 38:1, 275-301

To link to this article: http://dx.doi.org/10.1080/15421407708084393

Mol. Cryst. Liq. Cryst., 1977, Vol. 38, pp. 275–301

Printed in Holland

Optical Study of a Chiral Smectic C Under Shear

PAWEL PIERAŃSKI, ETIENNE GUYON, PATRICK KELLER and LIONEL LIÉBERT

Laboratoire de Physique des Solides associé au CNRS, Université Paris-Sud, 91405 Orsay

and

WOJCIECH KUCZYŃSKI and PIOTR PIERAŃSKI

Physics Institute of Polish Academy of Sciences, Poznań, ul. Smoluchowskiego 17/19

(*Received October 25, 1976*)

We study the distortion of a chiral smectic C, under a shear applied parallel to the plane of the layers, using an original technique based on the modification of the conoscopic image. Both the amplitude of the distortion and the phase lag between the alternating applied shear and the deformation are found to vary like the flow induced transverse polarization (described in Ref. 7). The behaviour is understood in terms of a viscoelastic–nematic-like model and of a simplified optical description which gives account of the displacement without deformation of the conoscopic image.

I INTRODUCTION

In a review talk at the 1976 Liquid Crystal Conference, Meyer[1] has given an extensive description of the experimental evidence of the existence of ferroelectricity in chiral smectic C (Sm C*) liquid crystals. The experimental effort in the last two years has followed the initial prediction and identification[2] of this phase on *p*-decyloxybenzilidene *p*-amino 2 methyl butyl cinnamate (DOBAMBC). Figure 1 gives the formula and indicates the site of the asymmetric carbon as well as the transverse dipole. It also gives the range of existence of the various phases. Below the smectic C* phase a chiral smectic H phase is also obtained which should also display ferroelectricity. The properties of this latter phase are not considered in the present work. In the Sm C* phase, the chiral molecules are organized in smectic C type layers which are optically biaxial.[3] As pointed out by Meyer, due to the reduction

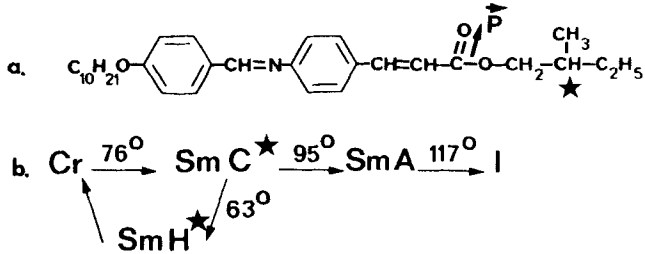

FIGURE 1(a) Extended formula of DOBAMBC. The site of the asymmetric carbon (*) and the transverse dipolar momentum are indicated. (b) Phase diagram of DOBAMBC. The smectic C* to smectic A transition is second order. Smectic C* and smectic H*, which is obtained only in decreasing temperature, can display a ferroelectric behavior.

of symmetry caused by the chirality of the molecule from the monoclinic one in the smectic C phase, a polarization can develop in the plane of the layer in a direction perpendicular to the molecules. However, the chirality also induces the smectic orientation, and subsequently the polarization, to rotate from one layer to the next. A full turn takes place over a macroscopic distance (the pitch p along the axis z perpendicular to the layers is of the order of a few microns)[4] (Figure 2a). Consequently, over the thickness of a typical

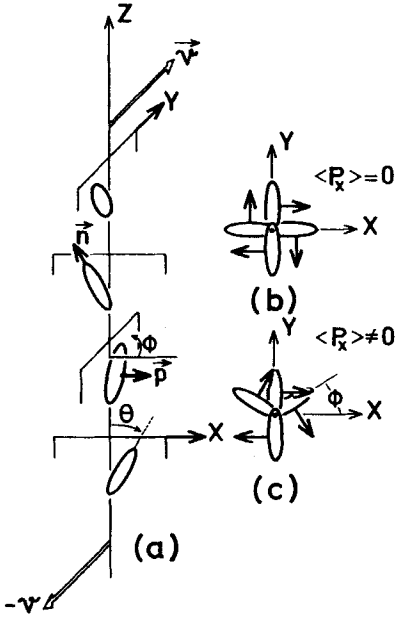

FIGURE 2(a) Schematic of the chiral smectic C* structure with the direction of the shear indicated. Top view of the structure without (b) and with (c) an applied shear. An average transverse dipolar momentum $\langle P_x \rangle$ across many layers develop under the influence of the shear.

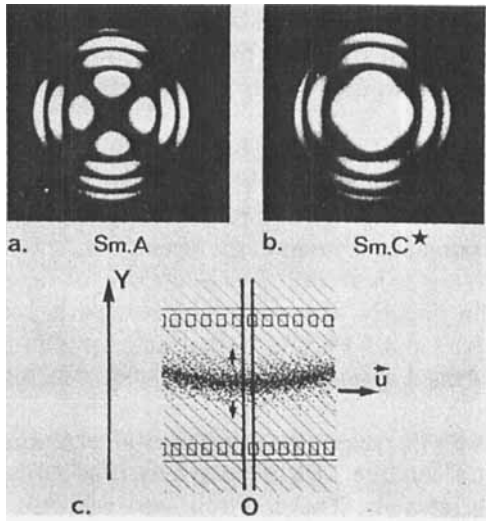

FIGURE 3 Conoscopic image in the smectic A (a) and C* (b) phase of DOBAMBC. The existence of rotatory power in (b) is seen from the clear central region. (c) schematic of the photographic detection of the displacement of the conoscopic image. The alternating displacement of a fringe of Figure (b) along the direction y of the shear is recorded on a photographic film, moving at a velocity U, through a narrow slot opening 0.

sample, $d \sim 200\ \mu$, there is no net polarization. A conoscopic image, formed in monochromatic light converging on the sample centered around z axis, also does not show any symmetry. The photographs of Figure 3 give the image obtained on DOBAMBC in the Sm C* phase at $T = 80°C$. This figure is very similar to that obtained in optically active α quartz.[5] It is compared with the corresponding image at $T = 95°C$, in the smectic A phase (the second order transition from Sm C* to Sm A is obtained at $T_{CA} = 95°C$). The two figures are fairly similar except near the central beam, due to the influence of chirality in the Sm C* regime.

In order to develop a net polarization, one can apply an electric field parallel to the layer.[2,6] We have obtained a similar effect by shearing the layers of a material contained between two plates perpendicular to the pitch axis, in a simple flow experiment.[7] The top view of Figure 2 shows the polarization and projection of the molecular alignment in the absence (b) and under the influence (c) of a shear. Due to the effect of flow alignment in (c) a component of the polarization appears along the direction x perpendicular to the velocity. In Ref. 7 this effect was detected using a capacitive technique. A nematic like hydrodynamic description was found to give a good account of this effect.

In order to get a closer approach of this shear induced ferroelectric behavior, we have decided to study the distortion of the Sm C* from the modification of the conoscopic image in a shear. This is the object of the present article.

If a small alternating shear is applied, the conoscopic image moves back and forth along the direction of the velocity—apparently without any distortion. Figure 4 is a photograph where the displacement of the dark fringe taken from a rectangular opening in the screen where the conoscopic image is formed (see Figure 3) is recorded as a function of time by displacing the photographic film linearly with time. The two parts correspond to shear frequencies $f = 0.57$ and 1 Hz and to the same amplitude of displacement. The amplitude of the displacement of the light spot increases with the shear rate.

In Section II, we will present the experimental techniques used. Instead of the photographic technique, we have used a more sensitive one using recordings of photocell intensity. The flow cell used will also be described. The results of our measurements on DOBAMBC are reported in Section III. We study the effect of the temperature and that of the frequency of the oscillation. By mixing the chiral product with its racemic, it is possible to increase the pitch p. We will show qualitatively the effect of the change of p and will postpone a report on a more quantitative study. Section IV will present a simplified model which explains the general features of the optical study in terms of the viscoelastic properties of the phase. Such a model rests heavily on the optical description of the propagation of oblique light in the chiral

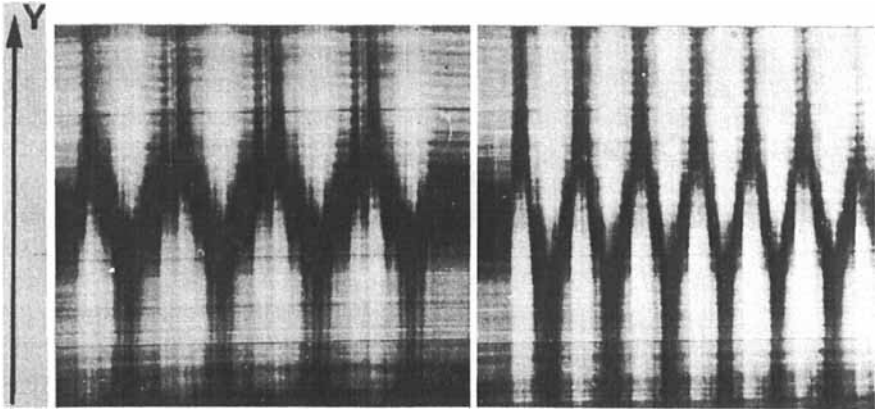

FIGURE 4 Using the technique of Figure 3c the displacement of the conoscopic image is recorded for the same displacement $x_0 = 1.24$ mm on a 240 μm thick film for two frequencies $f = 0.57$ (left) and 1 Hz (right). Results with this technique are consistent with those obtained with the photocell detection technique.

material in the absence or presence of a periodic distortion. An exact description involving a numerical evaluation will soon be available.[8b] We give in Appendix I a simplified description of the optics where the effect of rotatory power and birefringence are evaluated separately. Appendix II describes the electronics around the photocell detection.

II EXPERIMENTAL SET UP

1 Flow cell

The flow cell is represented on Figure 5. The liquid crystal is contained between two circular glass plates (1 cm diameter), distant of $d = 200$ to $300\,\mu$m which are part of a cylindrically shaped metallic internal oven (I.O.) made of two parts on which the glass plates are rigidly fixed.

The temperature of the oven is monitored by a platinum thermistance (T.R.) and regulated by supplying a power to the heating resistors (H.R.) via an electronic regulation. The temperature accuracy is of the order 10^{-2}K. In

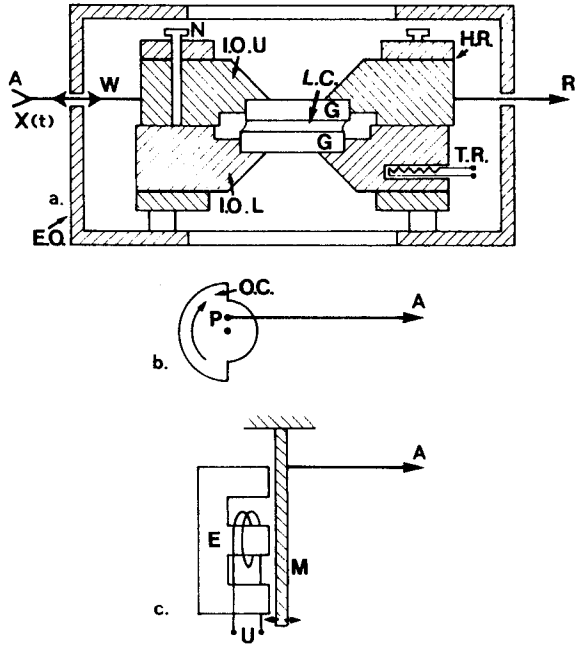

FIGURE 5(a) Schematic of the flow cell. The liquid crystal (L.C.) contained between the two coated glass plates (G) is sheared by moving the upper block (I.O.U.) parallel to the fixed lower one (I.O.L.) using the wire (W) coupling. Mechanical action on the wire for low frequency (b) and higher frequency (c) alternating excitation.

order to attain such a stabilization, the internal oven is surrounded by a second one (E.O.) which is maintained at a slightly lower temperature with an accuracy of 10^{-1}K.

The upper part of the internal oven (I.O.U.) is maintained on the lower one (I.O.L.) by three nylon screws (N) but can slide easily on it.

The inner faces of the glass plates (G) are coated with an orienting surfactant agent (CTAB)[9] which provides a homeotropic orientation in the smectic A phase. It has been found experimentally that, in the Sm C* phase, the smectic planes remain parallel to the glass plates.

2 Production of the oscillation motion

The oscillating motion is induced by a wire (W) coupled to a pin (P) attached excentrically on a rotating plate (Figure 5b) ($\omega_{max} \cong 2\pi \cdot 20$ Hz) or to a flexible magnetic rod (M) excited by a small electromagnet (E) (Figure 5c) ($\omega_{max} \cong 2\pi \cdot 200$ Hz).

The knowledge of the phase of the oscillating motion is required in the experiment.

In the case of the excitation by the excentric pin, this information is provided by an optical chopper (O.C.) coupled with the plate on which the pin is fixed. For the frequencies larger than 10 Hz, generated by the electromagnetic vibration, there is in general a phase lag between the supply voltage $U(t)$ and the displacement $x(t)$. This is due to the mechanical resonance of the system which occurs at the frequency ≈ 40 Hz. In this case, the phase of $x(t)$ is found by the following method:

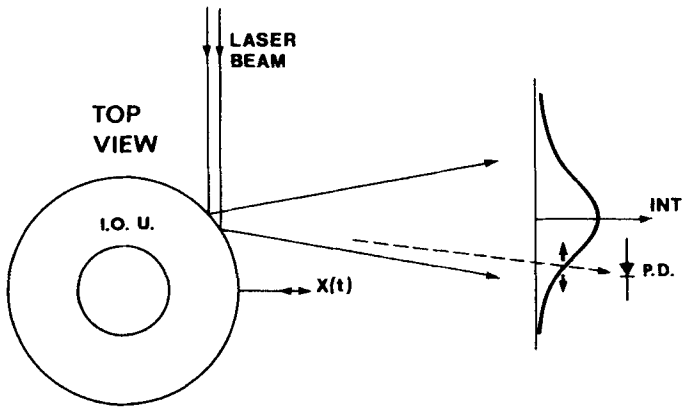

FIGURE 6 The amplitude and phase of the displacement $x(t)$ of the upper block (I.O.U.) are detected using a photodiode (P.D.) located in the region of largest slope of the reflected intensity of laser beam.

A laser beam is reflected by the cylindrical surface of the internal oven (Figure 6). A photodiode (P.D.) is positioned to read the intensity along the direction of the maximum slope of the gaussian distribution at the reflected light intensity. The displacement of the oven produces an overall rotation of the reflected beam and an alternating signal at the photodiode in phase with the displacement $x(t)$.

3 Optical detection

The system of the optical detection is represented on Figure 7.

The laser beam is channeled to the sample by an optical fiber (O.F.). It is subsequently polarised by the polariser (P) and focussed on the (L.C.) sample using a microscope objective (M.O.) of large frontal length (UMK 20 of Leitz).

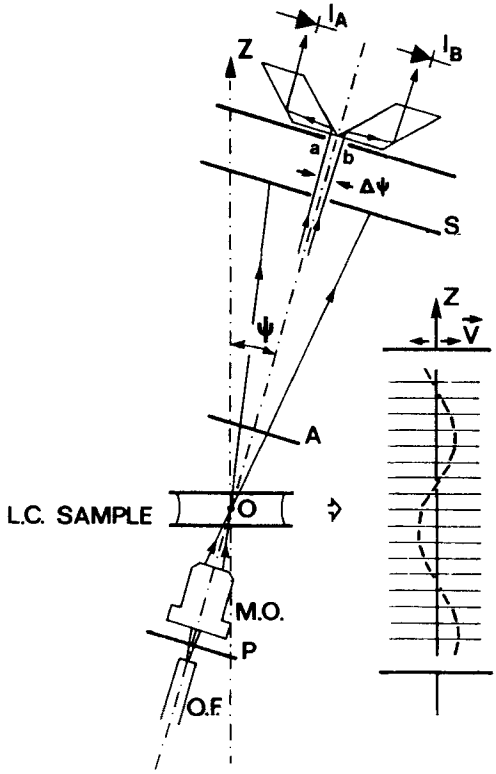

FIGURE 7 The optical detection system rotates as a whole around the center of the fixed sample cell. Intensities I_A and I_B are recorded as a function of the angle ψ of tilt with the normal to the layers. Note the double prism arrangement to separate the signals in the two close domains a and b ($\Delta\psi \sim 0.4°$).

The light cone going out of the sample is projected, across the analyser (A) (crossed with (P)), on a semitransparent screen (S), situated at a distance of 165 mm from the sample; the conoscopic figure is formed.

The screen (S) can be replaced by a system consisting of two prisms and two photodiodes (United Detector PIN 10 DP) which record the average intensities I_A and I_B of the light in two close rectangular sections a and b, (1 mm × 10 mm) of the conoscopic image. The fixed angle between the centers of a and b, $\Delta\psi \approx 0.4°$.

The optical system can rotate as a whole around the axis O parallel to the (L.C.) film and passing through the center of the cell. The angle ψ is detected by a potentiometer which is mechanically coupled to the rotation of the optical system and which delivers a voltage proportional to the angle ψ. This optical system allows us:

i) to detect the intensity of light in the conoscopic figure as a function of the angle ψ; $I = I(\psi)$ (using I_A, I_B or $I_A + I_B$).

ii) to measure the displacement of the conoscopic figure $\delta\psi$ which takes place when the shear is applied. In order to determine this displacement we must know the amplitude of oscillations of the light intensity (δI) seen by the photodiodes and detected accurately using a HR 8 lock-in amplifier (Appendix II). (The shear is always small enough so that the displacement $\delta\psi$ corresponds only to a very small fraction of an interfringe). The displacement will be $\delta\psi = \delta I/(dI/d\psi)$ where the local slope of intensity $dI/d\psi$ has to be measured independently. The slope can be found by two methods. The first one consists in measuring the difference $I_A - I_B$ which is proportional to the slope $dI/d\psi$ under the condition that the two channels A and B are balanced (Figure 8):

$$\frac{dI}{d\psi} = \frac{I_A - I_B}{\Delta\psi}$$

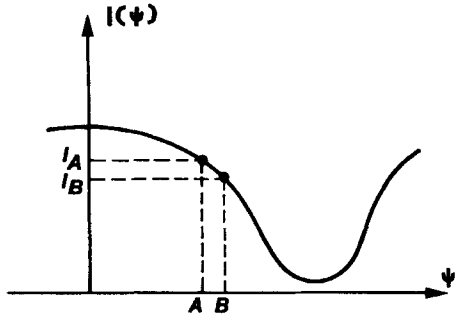

FIGURE 8 Principle of the detection of the displacement $\delta\psi$ of the conoscopic image. The slope $dI/d\psi$, where dI is the amplitude of variation of intensity of a photodiode in A (or B), is measured by the ratio $(I_A - I_B)/\Delta\psi$ where $\Delta\psi$ is the fixed angle between photocells A and B.

The second method consists in recording the intensity $I(\psi)$. The slope is determined graphically from this plot.

Typical results are given on Figures 11 and 12 in the next Section where we will discuss the practical use of these two methods.

In Appendix II we describe the electronic system which we use to supply the photodiodes and for the treatment of the information (phase sensitive detection and formation of $I_A + I_B$ and $I_A - I_B$ signals).

4 Microinterference noise suppression

The conoscopic figure is a superposition of the useful interferences due to the birefringence of the sample and of the detrimental microinterferences produced by the optical fiber, the imperfections in the monocrystalline sample and the dust particles. Due to the finite surface of the rectangular slots which delimit the portion of the conoscopic image seen by the photodiodes, these microinterferences are partially integrated. Nevertheless, a much more efficient method of integration[10] has been used in our experiments. The flexible optical fiber is shaken at low frequency (≈ 2 Hz) so that the microinterference pattern varies continuously. The noise signal due to this agitation can be suppressed through a low-pass filter (when the measurements $I(\psi)$ are performed) or by the lock-in amplifier (in the case of the measurements of the amplitude $\delta\psi$).

III RESULTS

Before reporting the central results of this work concerning the deformation of the conoscopic image under a shear, we think it useful to mention some observations on the general aspect of the conoscopic image produced by a typical sample 200 μm thick. In fact, these observations are of prime importance for the model of the light propagation in the Sm C* phase (developed in the Appendix I), which in turn is used to interpret the deformation of the conoscopic image induced by the shear flow.

1 Conoscopic image-General

Figure 9 gives the variations of intensity of light $I(\psi)$, recorded as a function of angle ψ, using the detection technique described in the Section II. This is the variation of intensity which would be obtained along the axis y of the conoscopic photographs (Figure 3). At 95°C, the DOBAMBC is in the Sm A phase and the plot $I(\psi)$ is characteristic of the uniaxial crystal.

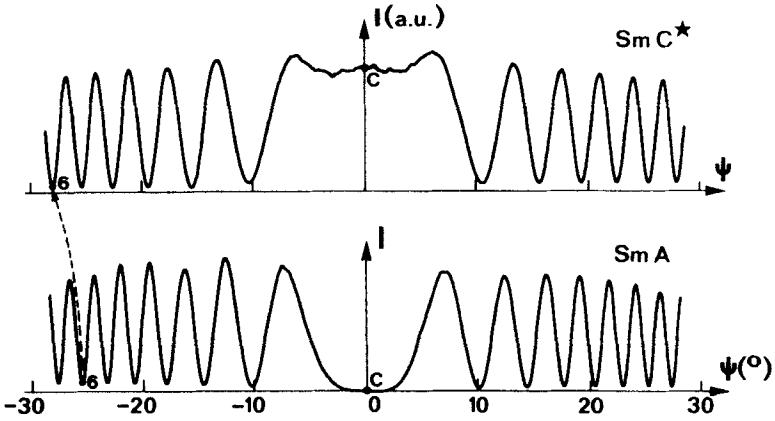

FIGURE 9 Variation of intensity $I(\psi)$ in the smectic A and C* phases (without shear) corresponding to that obtained in the photographs of Figure 3a and b taken along axis y. Direct recordings are used in this figure as well as in Figure 11 and 12.

When cooling down into the Sm C* phase (and even further into the Sm H* phase), we observe essentially two effects:

1a Rotatory power Intensity appears in the center of the conoscopic figure (c) progressively when decreasing the temperature and keeping the polarizers at right angle. At 80°C, the light intensity is almost at maximum. By rotating of the analyser (A on the Figure 7) in the clock-wise direction

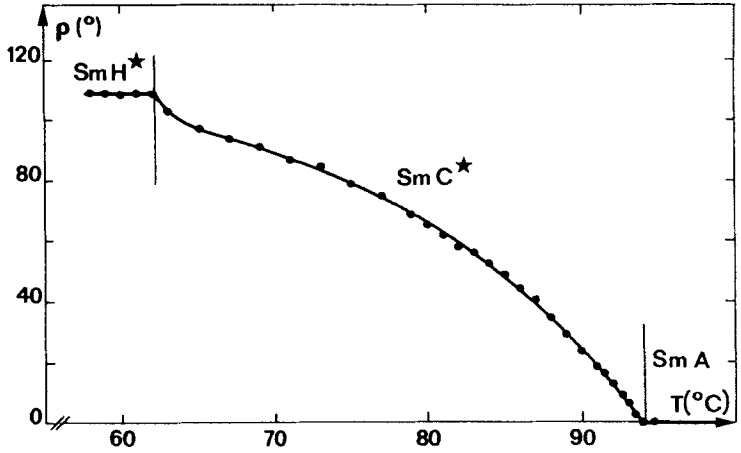

FIGURE 10 Rotatory power ρ in the smectic C* and H* phases. The progressive variation to zero next to the smectic A phase can be associated with that of the order parameter θ and is used to characterize the transition temperature T_{CA}.

(when looking at the sample from above) one can recover the extinction of light in the center of the image. The rotatory power measured by such a method is given as a function of the temperature on the Figure 10.

1b Birefringence Apart from the effect of the rotatory power in the central part of the image, the conoscopic figure in the Sm C* phase is very similar to that of the uniaxial smectic A phase. In other terms, this means that, from the point of view of light propagation, the smectic C* phase behaves approximately like some equivalent uniaxial material. Following such a model, we deduce that the effective birefringence decreases, when the sample is cooling down, from the observation that the diameter of the interference rings increases (see for example the sixth fringe on Figure 9).

2 Deformation of the conoscopic figure in the presence of the shear

2a General When an alternating shear flow is applied, the conoscopic figure also oscillates. In order to determine the amplitude of the oscillations, we used two methods described in Section II.3.

A typical recording of the first type is given in Figure 11. The upper curve gives the signal detected by the lock-in amplifier at the frequency of the shear, using $I_A + I_B$ as the input. The lower one is the difference between the two

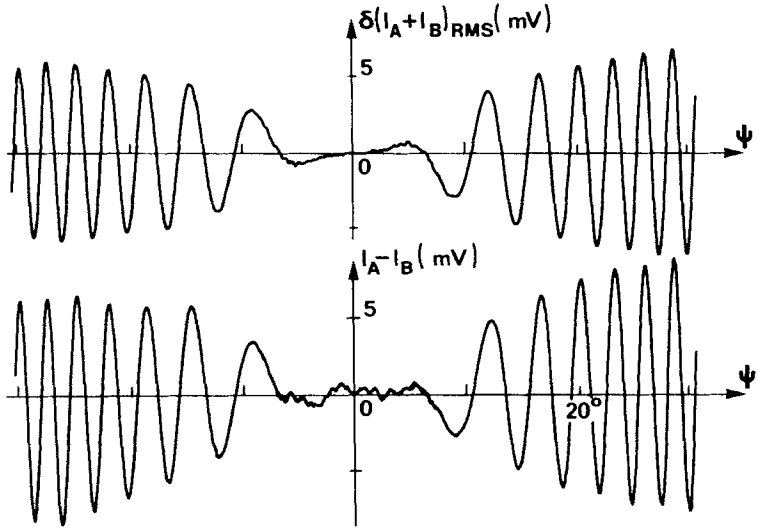

FIGURE 11 The upper part gives the amplitude of the intensity modulation in shear detected from a lock-in amplifier. The signal $I_A + I_B$ (as constructed in Figure 17) was used. The lower part gives the signal difference $I_A - I_B$. The balance between the two photodiodes was obtained independently.

photocell readings $I_A - I_B$; A balance of the two signals I_A and I_B has been obtained precisely electronically using potentiometer P on Figure 17 in Appendix II.

The extremums of both variations are in agreement with each other as expected.

From the ratio of the two signals and from $\Delta\psi$, we get the displacement

$$\delta\psi = \frac{\Delta\psi}{I_A - I_B}\,\delta(I_A + I_B)$$

A typical recording using the second method is given on Figure 12. We have recorded simultaneously both:

i) the signal δI_{rms} detected by the lock-in amplifier with I_A or I_B as an input.

ii) the intensity $I = I_A$ or I_B filtered by the low pass filter.

The extremums of the signal δI from the lock-in correspond to the extremum slopes on the $I(\psi)$ plot.

Let us note that, in practice, some difficulties can occur and perturb the data. The most frequent one is the buckling instability[11] which takes place when the displacement of the moving plate is large enough (≈ 1 mm). This phenomenon can be explained by a possible wedge shape of the sample, which gives rise to a dilation of the (L.C.) when the limiting plates move with respect to one another.

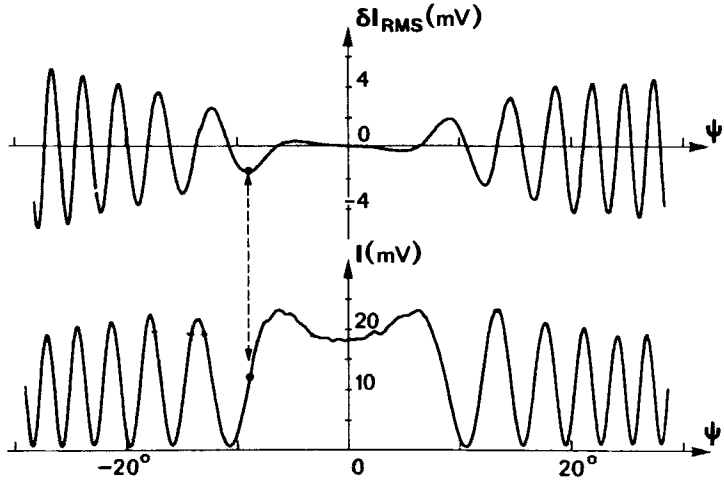

FIGURE 12 The lower part is similar to that given in Figure 9 in the Sm C* range. The upper part, the same as that in Figure 11, is proportional to the derivative $dI/d\psi$ of the lower one. Normalization of the upper curve is obtained from the value of the maximum slope in the lower graph.

We have avoided this difficulty by keeping a good parallelism of the limiting plates as well as by keeping a small amplitude x_0.

The buckling instabilities also occur when the temperature of the sample is changed suddenly or during the Sm A → Sm C* transition.

These structures relax spontaneously as soon as the temperature is stabilized.

2b Is the conoscopic image oscillating as a whole? This question is a crucial one for both practical reasons as well as for theoretical interpretations.

The test which has been performed consists in measuring the amplitude δI and the slope $dI/d\psi$ for different values of the exploration angle ψ (different regions of the conoscopic image). The plot of the results on Figure 13 shows a linear dependence between δI and $dI/d\psi$ and therefore gives the positive answer to this question (in the limit of available angles $|\psi| < 30°$).

Apart from the obvious practical simplification of the measurements, this result has an implication at the level of the theoretical description. It suggests that, in the presence of the shear, the conoscopic image deformation is like that which corresponds to the tilt of the optical axis in a uniaxial material. Such an hypothesis will be reexamined in the theoretical Section IV.

2c Temperature dependence The Figure 14 gives the variation of the amplitude of oscillations δI as a function of the temperature for a typical sample

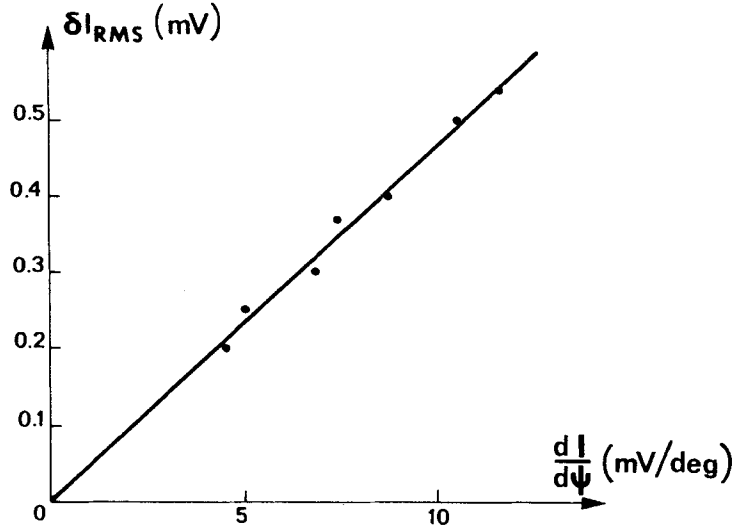

FIGURE 13 A linear relation is obtained between δI and $dI/d\psi$ (see the arrows on Figure 12) over the maxima detected for ψ below 30°. This indicates that the conoscopic image moves as a whole when the shear is applied.

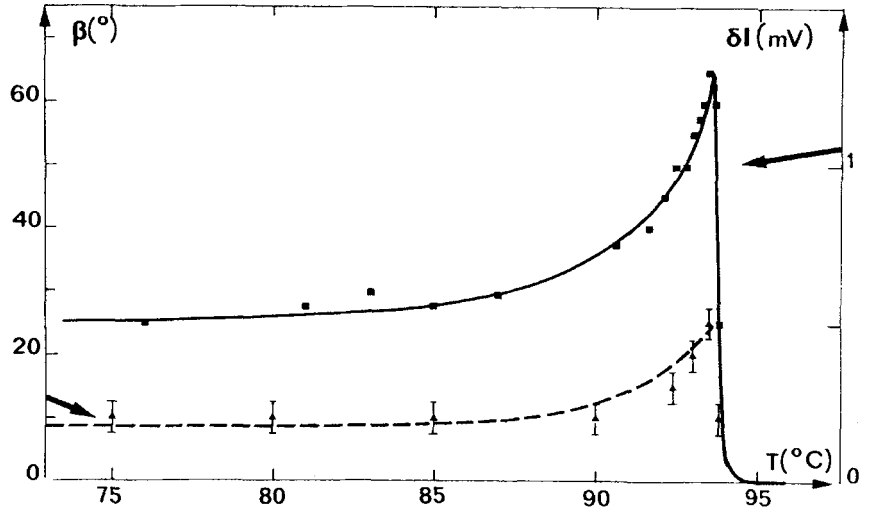

FIGURE 14 The temperature dependence of the intensity modulation recorded for a constant angle ψ (around the point of maximum slope of the $\delta I(\psi)$ curve) indicates a variation identical to that reported for the polarisation $\langle P_x(T)\rangle$ in Ref. 7. The temperature variation of the phase lag between $x(t)$ and the displacement $\delta I(t)$ also follows the same variation.

200 μm thick. The frequency of the shear has been kept constant: $f = 160$ Hz. (The measurement was made while sitting around the same interference fringe. If we neglect the small temperature dependence of the slope $dI/d\psi$ next to the transition the variation reflects well that of $\delta\psi$).

The most striking feature of this plot is that the amplitude of the oscillations increases in a singular manner in the vicinity of the Sm A $\rightarrow$ Sm C* transition. This variation is very similar to the temperature variation of the polarisation $\langle P_x(T)\rangle$ induced by shear, reported in Ref. 7. It suggests to us that the two signals ($\delta\psi(T)$ and $\langle P_x(T)\rangle$) are proportional to each other.

We will see in the Section IV that the theory confirms such a relationship.

In turn, the theory predicts another proportionality relationship between the amplitude of the oscillations $\delta\psi$ and the phase lag angle β between the excitation and response signals (in the low frequency limit). Following this suggestion we have also measured the phase lag β as a function of the temperature; the results are plotted on Figure 14. The temperature variation is indeed consistent with that of $\delta\psi$.

2d Frequency dependence Using the two systems of excitation described in the Section II.2 we have performed a study of the variation of the response with the frequency for a sample at 80°C.

At low frequency (< 10 Hz) the excitation ($\dot{x}(t)$) and the response ($\delta I(t)$) signals are practically in phase. At higher frequencies (up to 200 Hz), produced by the electromagnetic vibrator, a phase lag can be observed. It is plotted on Figure 15; at the maximum frequency 200 Hz it is of $13.5° \pm 2.5°$.

The accuracy of our measurements on β is limited by that of the phase sensitive detector (the reading accuracy is $\pm 2.5°$). On the other hand, there is an inherent limitation due to the large noise signal produced by the light diffusion on the dust particles and imperfections of the sample which are moving with the same frequency as that of the useful signal. It is interesting to note that, as far as the measurement of phase lag is concerned, the use of an electric field is better than that of the shear flow. Here are no moving parts and the noise to signal ratio is much better (see for example the Garoff communication in the Kent meeting[12]).

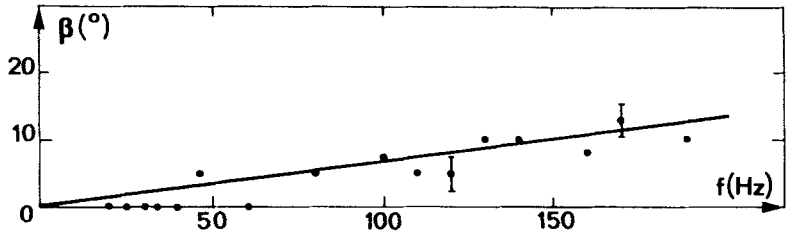

FIGURE 15 A linear relation is obtained between the phase lag β and the shear frequency f, as expected in the low frequency limit. Note the large error bars due to the parasitic signals involved in a moving plate experiment.

The amplitude of the response δI detected by the lock-in amplifier varies with the frequency similarly to the phase lag. If we keep the displacement x_0 constant, we observe (Figure 16) that the amplitude δI is proportional to the shear rate in the available frequency range.

2e Concentration dependence By mixing the pure chiral product with its racemic, we can change continuously the pitch of the helix and, consequently, the properties of the Sm C* phase.

We have made the following qualitative observations on experiments performed in the same conditions (temperature, frequency, shear rate):

i) the amplitude of the oscillations $\delta\psi_0$ is larger in the sample with the smaller chiral concentration (larger pitch)

ii) the phase lag between the excitation and the oscillation of the conoscopic figure increases with the pitch of the helix.

Let us note that a good conoscopic image is difficult to obtain for the sample with a small concentration of the chiral product. In fact, it is well known

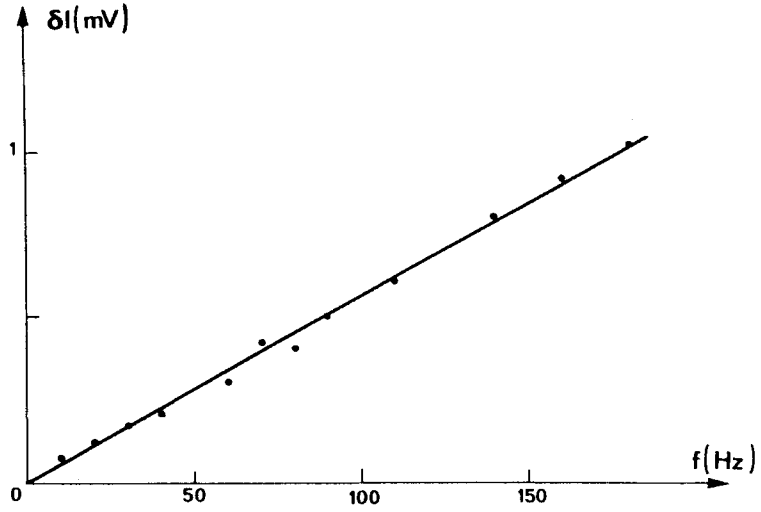

FIGURE 16 A linear relation is also obtained between the displacement of the image and frequency.

that it is difficult to obtain a well aligned-single domain-sample with a pure racemic (Sm C) material.

IV DISCUSSION

1 Helix distortion and its relationship with the deformation of the conoscopic image

1a Distortion induced by the shear (small perturbation limit) Locally the chiral smectic C phase is biaxial. The spatial orientation of the corresponding dielectric susceptibility ellipsoid can be described by three angles θ, ϕ, η. In the frame of reference such that z axis is normal to the smectic layers, η is zero, θ is constant and ϕ varies linearly with z; $\phi(z) = 2\pi z/p$. (Figure 2a).

We suppose that, when the shear is applied, only the angle ϕ is affected. This angle corresponds to the phase of the smectic C order parameter[14] and has a hydrodynamic behaviour[15] in contrast with the absolute value of the order parameter θ which will be supposed to remain constant under shear.

If we neglect the velocity profile due to the existence of the helix and to its distortion, we have to consider only an equation of motion for the angle ϕ

$$B_3 \frac{d^2\phi}{dz^2} - \gamma\dot{\phi} = -\alpha \frac{v \cos \phi}{d}; \qquad (1.1)$$

$$v = v_0 e^{j\omega t}$$

The first term gives the elastic torque which opposes the distortion from the static configuration $\phi = qz$ ($q = 2\pi/p$). The elastic coefficient B_3 is defined in Ref. 14 (form 7.61). The second term accounts for the rotational viscosity. The term on the right hand side gives the driving torque of the alignment proportional to the viscosity coefficient $\alpha = \gamma \cdot \lambda^1$ where γ and λ^1 are defined in the hydrodynamic description of smectics in Ref. 15.

In the approximation of small perturbations the destabilizing torque $\alpha(v/d)\cos\phi$ will excite the perturbation modes of the same spatial and temporal periodicity. The helix configuration distorted by the flow can be written as

$$\phi(z, t) = qz + \phi_0 e^{j(\omega t + \beta)} \cos qz \tag{1.2}$$

Inserting this expression in the equation of motion (Eq. 1.1), one can calculate the amplitude of distortion

$$\phi_0 = \frac{\alpha}{\gamma} \frac{1}{\sqrt{\omega^2 + (1/\tau)^2}} \frac{v}{d} \tag{1.3}$$

and the phase lag β between the distortion and the excitation.

$$\beta = -\tan^{-1}(\omega\tau) \tag{1.4}$$

The time

$$\tau = \frac{\gamma}{B_3 q^2}$$

is a characteristic time of relaxation of the distortion.

1b Relationship between the helix distortion and the deformation of the conoscopic image The deformation of the conoscopic figures due to the distorsion of the helix in the shear flow, will be described in the following by means of the theoretical model, used in Appendix I in order to explain the general features of the conoscopic figure in a Sm C* single crystal. The main assumption of this model is that one can separate two contributions in the conoscopic image like it is done usually in the case of uniaxial crystals with optical activity:[13]

i) rotatory power

ii) uniaxial birefringence.

In order to estimate the contribution of the uniaxial birefringence, we calculate in Appendix I the form of the average dielectric susceptibility tensor $\hat{\varepsilon}_0 = \langle \hat{\varepsilon}(z) \rangle$, which appears to be a uniaxial tensor with the principal axis parallel to the axis of the helix as observed experimentally (see the uniaxial symmetry of the conoscopic photograph, Figure 3).

On the other hand, the rotatory power in the center of the conoscopic image is explained in terms of Parodi's[16] analysis, which reduces the problem of light propagation in the Sm C* phase to that in the cholesterics analyzed originally by de Vries,[17] provided some new effective indices $\tilde{\tilde{n}}_0$ and $\tilde{\tilde{n}}_e$ are introduced. We have to consider the effect of the helix distortion on both the normal birefringence and the rotatory power, which contribute together in the conoscopic figure.

The experimental observations (Section III.1) suggest that the main contribution will be that of the normal birefringence; in fact, one observes that the conoscopic figure is moving as a whole when the shear is applied. Following the results of Ref. 18, the overall displacement of the conoscopic image is found to correspond to the inclination of the effective optical axis (principal axis of the tensor $\langle\hat{\varepsilon}\rangle$).

This assumption is in fact verified by the calculation of the average dielectric susceptibility tensor $\hat{\varepsilon}_0$ (defined by the Eq. A2.1) for the helix configuration perturbed by the flow (given by the Eq. 1.2).

Following the computational schema of Appendix I and retaining only the terms of first order in ϕ_0, one obtains:

$$\langle\hat{\varepsilon}\rangle = \hat{\varepsilon}'_0 = \begin{pmatrix} a & 0 & 0 \\ 0 & a & \delta \\ 0 & \delta & b \end{pmatrix} \tag{1.6}$$

where $a = \varepsilon_1 + \frac{1}{2}(\varepsilon_3 - \varepsilon_1)\sin^2\theta + \frac{1}{2}(\varepsilon_2 - \varepsilon_1)$

$$b = \varepsilon_1 + (\varepsilon_3 - \varepsilon_1)\cos^2\theta$$

$$\delta = (\varepsilon_3 - \varepsilon_1)\tfrac{1}{2}\phi_0 e^{j(\omega t + \beta)} \sin\theta\cos\theta$$

The form of this tensor indicates that its long axis is no longer parallel to the z direction as in the non perturbed configuration for which we had (Eq. A2.2):

$$\hat{\varepsilon}_0 = \begin{pmatrix} a & 0 & 0 \\ 0 & a & 0 \\ 0 & 0 & b \end{pmatrix} \tag{1.7}$$

In the approximation of small distortions, one finds that the rotation around the x axis, characterized by the tensor $\hat{T}$, about the angle $\xi(\xi \ll 1)$ applied to the tensor $\hat{\varepsilon}_0$, transforms it to the form

$$\hat{T}\hat{\varepsilon}\hat{T}^{-1} \cong \begin{pmatrix} a, & 0, & 0 \\ 0, & a, & (b-a)\xi \\ 0, & (b-a)\xi, & b \end{pmatrix} \tag{1.8}$$

This is identical with the form of the tensor $\hat{\varepsilon}'_0$ (Eq. 1.6) calculated for the configuration perturbed by the flow.

By identification

$$(b - a)\xi = \delta \tag{1.9}$$

we find:

$$\xi_0 = \tfrac{1}{2}\phi_0 \frac{(\varepsilon_3 - \varepsilon_1)\sin\theta\cos\theta}{(\varepsilon_3 - \varepsilon_1)\cos^2\theta - \tfrac{1}{2}(\varepsilon_3 - \varepsilon_1)\sin^2\theta - \tfrac{1}{2}(\varepsilon_2 - \varepsilon_1)} \tag{1.10}$$

This formula simplifies a lot in the small tilt angles ($\theta \ll 1$):

$$\xi_0 = \tfrac{1}{2}\phi_0 \sin\theta \tag{1.11}$$

On the other hand, the interference figure for a uniaxial crystal plate with the optical axis at an angle ξ with the normal to the plates is known.[18] In an approximation where the difference between the indices is small compared with their values, one finds that the birefringence evaluated in the plane of incidence is extremal for a normal to the waves in the crystal along the optical axis. The variation being symmetrical around this direction, one can deduce that for small angles the center of the conoscopic image will be tilted by an angle (evaluated outside of the sample)

$$\delta\psi_0 = \tilde{n}_0\xi_0 \tag{1.12}$$

$\tilde{n}_0$ being an effective ordinary index (Eq. A2.3).

We can conclude that the distortion of the helix

$$\delta\phi = \phi_0 e^{j(\omega t + \beta)}\cos qz \tag{1.13}$$

induces oscillations of the conoscopic figure in the direction of the flow

$$\delta\psi = \delta\psi_0 e^{j(\omega t + \beta)} \tag{1.14}$$

of amplitude

$$\delta\psi_0 = \tilde{n}_0\tfrac{1}{2}\phi_0 \sin\theta \tag{1.15}$$

2 Interpretation of the experimental results in terms of the viscoelastic behaviour of the Sm C* phase

2a Frequency dependence The phase difference β between the deformation of the conoscopic figure and the excitation (shear rate) has been observed experimentally to vary linearly with the frequency. These results are presented on Figure 15. Such a behaviour agrees with the theoretical Eq. 1.4 which, in the low frequency limit, predicts a linear variation $\beta(\omega)$.

The slope of the plot $\beta(\omega)$ leads to an estimate of the relaxation time

$$\tau = 1.9 \cdot 10^{-4}\ \text{sec}$$

Using the value of the pitch $p = 4\ \mu m$ from the Ref. 4, we calculate the ratio

$$\frac{B_3}{\gamma} = 2.2 \cdot 10^{-5}\ \text{(cgs)}.$$

No other measurements of B_3 and γ are presently available.

Nevertheless, and estimate of this coefficient can be made using an approximation of the type "uniaxial smectic C". In fact, if we neglect the biaxiality of the chiral smectic C phase, we can apply the formalism generally used for the description of the viscoelastic behaviour of the nematic phase (such an approximation is applied in Ref. (7)). In terms of this approximation, the ratio: B_3/γ can be written as:

$$\frac{B_3}{\gamma} = \frac{K_3 \sin^2\theta \cos^2\theta + K_2 \sin^4\theta}{\gamma_1 \sin^2\theta} \tag{2.1}$$

In the limit of small tilt angles θ we have

$$\frac{B_3}{\gamma} \approx \frac{K_3}{\gamma_1} \tag{2.2}$$

In a typical nematic we obtain an order of magnitude estimate

$$\frac{K_3}{\gamma_1} \approx \frac{10^{-6}}{10^{-1}} = 10^{-5}\ \text{cgs} \tag{2.3}$$

The value agrees with the ratio 2.2×10^{-5} cgs determined from the experiments. Independent measurements of these factors are desirable.

An interesting prediction of the Eq. 2.1 is that the ratio B_3/γ has a non singular behaviour at the Sm A–Sm C* transition. (Consequently, the temperature dependence of the relaxation time τ is determined by the variation of the pitch p).

In Section 2d we will discuss this variation more in detail. The experimental plot of Figure 16, which gives the amplitude of oscillations δl ($\sim \delta\psi$) as a function of frequency ω, has been obtained in the low frequency limit $\omega \ll 1/\tau$ for which the theoretical Eq. 1.3 and 1.15 give the following result:

$$\delta\psi_0 = \tfrac{1}{2}\tilde{n}_0 \sin\theta \cdot \frac{\alpha}{\gamma}\tau\frac{x_0}{d}\cdot\omega; \qquad \left(\frac{x_0\omega}{d} = \frac{v_0}{d}\right)$$

Qualitatively this formula explains the linear dependence $\delta\psi_0(\omega)$.

2b Numerical estimates Let us now estimate the displacement $\delta\psi_0$ given by this formula for the typical quantitative example where for $x_0 = 40\ \mu m$, $d = 200\ \mu m$, $\omega = 2\pi.30$ Hz we have measured $\delta\psi_0 = 0.35°$. The unknown factors are $\tilde{n}_0$ and $(\alpha/\gamma)\sin\theta$. We have measured $\tilde{n}_0$ at 80°C; $\tilde{n}_0 = 1.42$.

The factor $(\alpha/\gamma)\sin\theta$ can be estimated as in the previous section using the "uniaxial smectic C" approximation.

$$\frac{\alpha}{\gamma}\sin\theta = \frac{\alpha_2 \sin^2\theta\cos\theta}{\gamma_1 \sin^2\theta} \approx \frac{\alpha_2}{\gamma_1} \tag{2.4}$$

for small θ.

In nematics, α_2/γ_1 is known to be of the order of 1, except a special case of the vicinity of the Sm A–N transition, so that we can write

$$\delta\psi_0 \approx \tfrac{1}{2}\tilde{n}_0\tau s \tag{2.5}$$

where $s = x_0\omega/d$.

Finally, we calculate

$$\delta\psi_0 = 0.3°$$

to compare with the experimental value

$$\delta\psi_0 = 0.35°.$$

2c Temperature dependence The temperature dependence of the deformation of the conoscopic image $\delta I(T)$ represented on Figure 14 is identical to that of the shear flow induced polarisation P_x studied in Ref. 7 (Figure 4 of Ref. 7).

This similarity is explained simply by the fact that these two quantities are proportional to each other as we will see in the following. The Eq. 1.15 of the present work gives

$$\delta\psi_0 = \tfrac{1}{2}\phi_0\tilde{n}_0\sin\theta$$

while the Ref. 7 provides a relation between the average polarization $\langle P_x\rangle$ and the distortion:

$$\langle P_x\rangle_0 = \tfrac{1}{2}\phi_0 P_m f(\theta)$$

P_m is the permanent electric dipole per molecule and $f(\theta)$ represents an unknown function which relates the spontaneous polarisation per molecule P to the order parameter θ

$$P = P_m \cdot f(\theta)$$

For reasons of symmetry the lowest power term in the expression of $f(\theta)$ is linear in θ.

Consequently, in the limit of the small tilt angle, we have

$$\delta\psi_0 \sim \langle P_x\rangle_0$$

and, in the vicinity of the Sm A–Sm C* transition, we expect the plots $\langle P_x\rangle_0(T)$ and $\delta\psi_0(T)$ to be of the same shape.

2d Pretransitional behavior At the approach of the Sm C*–Sm A transition the response curve $\delta I(T)$ (Figure 14) shows a rather singular increase.

Theoretically, the Eq. 2.5 indicates that the role of the relaxation time $\tau(q)$ can be retained as a principal factor in the response function variation.

This assumption is confirmed by similar singular behaviour of the phase lag β (plotted on the same figure) which is a measure of the relaxation time of the helix distortion (Eq. 1.4).

This relaxation time τ being a product of two factors γ/B_3 and $1/q^2$ we we have to examine both terms in view of possible singular behaviour at the transition.

The first one γ/B_3 has been estimated previously in terms of a "uniaxial smectic C" type approximation (Eq. 2.1) and its contribution cannot explain the singularity because we see no fundamental reasons for the singular behaviour of γ_1 or of K_3.

We examine next the temperature variation of the pitch p. The available data[4] tell us that in DOBAMBC the pitch p which, in most of the temperature range is of the order of 4 μm, increases slightly at the Sm C* → Sm A transition; the limit value is 5 μm.

Such a small variation of the pitch cannot explain entirely the increase of the response at transition.

The explanation of this discrepancy we can foresee at present is an abnormal variation of the pitch when the sample is submitted to a shear (or to the electric field like in experiments reported in Ref. 4).

By analogy with the case of a cholesteric submitted to the magnetic field (the description of this problem is given for example in Ref. 14 Section 6.2.2) we know that the pitch of the helix can increase in a divergent manner close to the critical shear rate (or electric field intensity) above which the helix is completely unwound. Due to the variation of the tilt angle in the vicinity of the Sm C* → Sm A transition, the critical shear rate is expected to go continuously to zero at the transition. Consequently for all values of the driving shear rate, even for the smallest ones, the helix can be unwound if we are close enough to the Sm C* → Sm A transition. We have preliminary results on an experiment where the Sm C* material is submitted to a composite shear $v_x = a \cos \omega t$, $v_y = a \sin \omega t$. Next to the smectic A transition the helix can be completely unwound and we observe that a smectic C type conoscopic figure rotate as a whole at the frequency of the shear around the z axis.

V CONCLUSION

The present work can be pursued in several directions.

First of all, the pretransitional effects in the smectic A phase remain to be studied. It is known from Garoff experiments[12] that the electric field induces

a tilt angle in the Sm A phase; by analogy we should expect to observe such an effect under shear. Unfortunately, in the shear flow experiments the motion of imperfections in the single domain samples produces a very large parasitic signal and we have not yet been able to detect an appreciable precursory effect.

Another interesting extension of this optical study is the use of the informations about the helix deformation, which it provides, in order to obtain the spontaneous polarization by using the capacitive type measurement which can be performed at the same time as the optical study. Such a hybrid method could be very useful for the comparative study of the spontaneous polarisation in different smectic C* materials.

Finally, in other liquid crystal phases the application of the shear flow or any other periodic excitation can induce a perturbation, which could be detected by the sensitive optical technique developed in the present work. An interesting example of such an application is the measurement of the ratio α_2 (or α_3)/γ_1 in the nematic phase, which we intend to publish soon. (A typical result has already been shown on Figure 1 of Ref. 21).

Our interpretations rest on the viscohydrodynamic description carried as an extension of that of nematics. It is of great interest to develop independent measurements of the parameters involved. Torque determinations of the constant γ are being done in different groups.[22] We have neglected the contributions of the biaxiality, apart from that induced by the molecular tilt, in this description as well as in the optics. An exact numerical study where the contribution of the biaxiality (angle η) is retained is under way[8] and should help clarify this point.

Acknowledgements

This work has been done as a collaboration between Orsay and Poznan thanks to mutual visits of two of us. Lionel Liébert in Poznan, Piotr Pierański in Orsay. We acknowledge the support from the Polish Academy of Sciences and from C.N.R.S. This work has been partially supported by an A.T.P. of C.N.R.S. on instabilities. Discussions on the optics of chiral phases with D. Taupin are greatly acknowledged. We have had useful exchanges with Y. Galerne, S. Garoff, P. Martinot-Lagarde and L. Strzelecki.

References

1. R. B. Meyer, invited lecture at VIth Int. Conf. on L.C., Kent 1976.
2. R. B. Meyer, L. Liebert, L. Strzelecki, and P. Keller, *J. Physique Lett.*, **36** (1975) L-69.
3. T. R. Taylor, J. L. Fergason, and S. L. Arora, *Phys. Rev. Lett.*, **24** (1970) 359.
4. Ph. Martinot-Lagarde, Communication at Kent Conf. (76).
5. A. Sommerfeld, *Optics*, Academic Press, Inc., N.Y. (1954) §29 and Fig. 49.
6. Ph. Martinot-Lagarde, communication at Kent Conf.
7. P. Pierański, E. Guyon, and P. Keller, *J. Physique*, **36** (1975), 1005.
8a. D. Taupin, *J. Physique, Colloque C4 supplément*, **30** (1969) C4-32.

8b. D. Taupin, to be published.
9. I. Haller, *J. Chem. Phys.*, **57** (1973) 1400.
10. Y. Galerne, S. T. Lagerwall, and I. W. Smith, to be published in *Opt. Comm.*
11. M. Delaye, R. Ribotta, and G. Durand, *Phys. Lett.*, **A44** (1973) 139.
12. S. Garoff, communication at Kent Conf. (1976).
13. J. F. Nye, *Physical Properties of Crystals*, Chapter XIV, Oxford University Press (1957).
14. P. G. de Gennes, *The Physics of Liquid Crystals* (1974) Oxford Press.
15. P. C. Martin, O. Parodi, and P. S. Pershan, *Phys. Rev.*, **6** (1972) 2401.
16. O. Parodi, *J. Physique, Colloque C1, supplément of*, **36** (1975) C1-325.
17. H. L. de Vries, *Acta Crystallogr.*, **4** (1951) 219.
18. H. Born and E. Wolf, *Principles of Optics*, Pergamon Press (1964) §14.4.4.
19. M. Brunet, *J. Physique, Colloque C1, supplement of*, **36** (1975) C1-321.
20. D. W. Berreman, *Mol. Cryst. Liquid Cryst.*, **22** (1973) 175.
21. P. Pierański and E. Guyon, *Comm. on Phys.*, **1** (1975) 45.
22. P. J. Flanders, *Appl. Phys. Lett.*, **28** (1976) 571; S. Meiboom, communication at Kent Conf.
23. A. J. Diefenderfer, *Principles of Electronic Instrumentation*, W. B. Saunders Company (1972).

Appendix I On the light propagation in the Smectic C* phase

The propagation of light in a chiral material is fairly complex. In cholesterics, the classical de Vries analysis[17] for normal incidence beam has been followed by numerical studies of the reflection in oblique incidence.[8] Some extensions of these treatments for the case of Smectic C* are available.[20] We will distinguish between the normal and oblique incidence cases.

I CENTER OF THE CONOSCOPIC IMAGE

The exact solutions for the propagating modes have been given by Parodi.[16] He found that the de Vries analysis can be applied to Sm C* provided one uses the local effective refractive indices $\tilde{\tilde{n}}_e$ and $\tilde{\tilde{n}}_0$

$$\tilde{\tilde{n}}_e^2 = \frac{\varepsilon_1 \varepsilon_3}{\varepsilon_1 \sin^2 \theta + \varepsilon_3 \cos^2 \theta} \qquad \text{(A1.1)}$$

$$\tilde{\tilde{n}}_0^2 = \varepsilon_2$$

θ, the tilt angle, is the angle between the normal to the layers and the long axis ε_3 of the dielectric susceptibility tensor $\hat{\varepsilon}$.

The intermediate axis ε_2 is normal to the tilt plane. The optical behaviour is characterized by a reduced wavelength $\lambda' = \lambda/(p\sqrt{\varepsilon})$ of the order of 0.1; the laser wavelength is $\lambda = 0.6328\ \mu$m and $\varepsilon = (\tilde{\tilde{n}}_e^2 + \tilde{\tilde{n}}_0^2)/2$. Near the smectic

C* → Smectic A transition where the tilt angle is small as well as the biaxiality term $\varepsilon_2 - \varepsilon_1$ (the measurements of the biaxiality performed by Galerne *et al.*[10] indicate indeed that, for $\theta = 5°$, $\sqrt{\varepsilon_2} - \sqrt{\varepsilon_1} \cong 1.5 \cdot 10^{-4}$); the birefringence measured by $\tilde{\tilde{n}}_e^2 - \tilde{\tilde{n}}_0^2$ is small and in terms of de Vries analysis the propagating modes are nearly circulary polarized.

Due to the different velocities of the left and right normal circulating modes, there is an effective rotatory power which is given by the formula

$$\rho = -\frac{2\pi}{p} \frac{\alpha^2}{8\lambda'^2(1 - \lambda'^2)} \tag{A1.2}$$

where

$$\alpha = \frac{\tilde{\tilde{n}}_e^2 - \tilde{\tilde{n}}_0^2}{2(\tilde{\tilde{n}}_e^2 + \tilde{\tilde{n}}_0^2)}$$

In the Sm C* phase the rotatory power has been observed by Brunet[19] to be a function of temperature (see also the Figure 10 of the present work). The main contribution to this variation is the temperature dependence of the tilt angle θ. Using the Eq. (1.1) we find

$$\tilde{\tilde{n}}_e^2 - \tilde{\tilde{n}}_0^2 = (\varepsilon_1 - \varepsilon_2) + (\varepsilon_3 - \varepsilon_1)\frac{\varepsilon_1}{\varepsilon_3} \sin^2 \theta \tag{A1.3}$$

One can argue that for reasons of symmetry the biaxiality $(\varepsilon_1 - \varepsilon_2)$ should be a quadratic function of θ just as the second term in Eq. 1.3. Therefore, the rotatory power should be proportional to the fourth power of θ and consequently should vanish continuously at Sm C* → Sm A transition as observed experimentally.

II PERIPHERIC REGIONS OF THE CONOSCOPIC IMAGE

The exact solutions of the Maxwells equations for the light propagation at the oblique incidence is much more difficult to obtain. The Berreman's calculations relative to this problem[20] deal with the light reflection, while in the present work we are interested by the transmission of the polarized light.

The main difficulty is due to the complex form of the dielectric susceptibility tensor $\hat{\varepsilon}$ which is a periodic function of z.

In fact, the Berreman's calculations tell us that there are five Fourier components in $\hat{\varepsilon}$:

$$\hat{\varepsilon}(z) = \hat{\varepsilon}_0 + \hat{\varepsilon}_1 e^{-j(\phi/2)} + \hat{\varepsilon}_{-1} e^{j(\phi/2)} + \hat{\varepsilon}_2 e^{-j\phi} + \hat{\varepsilon}_{-2} e^{j\phi} \tag{A2.1}$$

where

$$\phi = qz = \frac{2\pi z}{p}$$

The average term $\hat{\varepsilon}_0$ has an uniaxial symmetry:

$$\hat{\varepsilon}_0 = \begin{pmatrix} \tilde{n}_0^2, & 0, & 0 \\ 0, & \tilde{n}_0^2, & 0 \\ 0, & 0, & \tilde{n}_e^2 \end{pmatrix} \tag{A2.2}$$

where

$$\begin{aligned} \tilde{n}_0^2 &= \tfrac{1}{2}(\varepsilon_1 + \varepsilon_2) + \tfrac{1}{2}(\varepsilon_3 - \varepsilon_1)\sin^2\theta \\ \tilde{n}_e^2 &= \varepsilon_1 \sin^2\theta + \varepsilon_3 \cos^2\theta \end{aligned} \tag{A2.3}$$

so that, in zero order approximation, the Sm C* behaves like an uniaxial crystal with effective indices $\tilde{n}_e^2$ and $\tilde{n}_0^2$.

For a beam incident under a small incidence angle ψ (not too small however in order to be able to neglect the contribution of the rotatory power) we get a phase difference between the ordinary and extraordinary rays:

$$\delta = \frac{\pi d}{\lambda}\tilde{n}_0\left(\frac{1}{\tilde{n}_0^2} - \frac{1}{\tilde{n}_e^2}\right)\sin^2\psi \tag{A2.4}$$

The enlargement of the diameter of the interference circular rings observed experimentally can be explained at present. If we suppose that the dielectric susceptibilities are not singular at the transition Sm A → Sm C, the phase difference δ for some constant angle ψ varies as a second power of the tilt angle

$$\delta = \delta_A - \alpha\theta^2$$

where δ_A refers to the phase difference in the Sm A phase and α is a positive factor.

Appendix II

Figure 17 represents the electronic circuit which has been used in experiments to supply the photodiode and to form the $I_A - I_B$ and $I_A + I_B$ signals.

The resistors 500 kΩ, in the feedback of the two μA 741 operational amplifiers on the left, define the sensitivity of photodiodes.

The two op. amp. on the right are connected in classical summation and differential operating configurations.

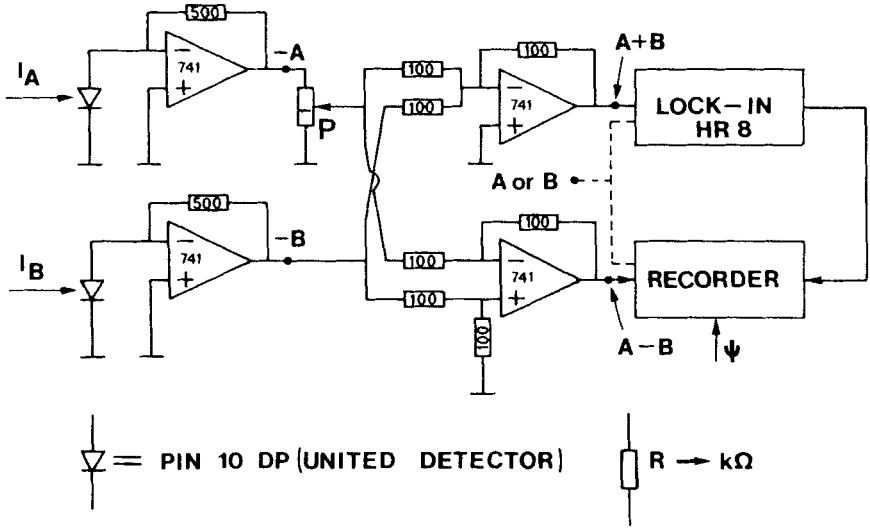

FIGURE 17 Electronics of the system used to add and substract the photocell signals I_A, I_B. The treatment of the signals obtained is also indicated.

The potentiometer P is used to equilibrate the A and B channels (the unbalance comes in particular from the difference in the area of the slits a and b (Figure 7) which delimitate the light intensity seen by the photodiodes).